

Robust Control of a Multifrequency Metamaterial Cloak Featuring Intrinsic Harmonic Selection

Yongjune Kim,^{1,2} Tianwei Deng,^{1,3} Wei Xiang Jiang,⁴ Tie Jun Cui,⁴ Yongshik Lee,^{5,*} and Cheng-Wei Qiu^{1,†}

¹*Department of Electrical and Computer Engineering, National University of Singapore, Singapore, 117583, Singapore*

²*Center for Advanced Meta-Materials, 156 Gajeongbuk-ro, Yuseong-gu, Daejeon 34103, South Korea*

³*Temasek Laboratories, National University of Singapore, Singapore 117411, Singapore*

⁴*State Key Laboratory of Millimeter Waves, Southeast University, Nanjing 210096, P. R. China*

⁵*Department of Electrical and Electronic Engineering, Yonsei University, Seoul 03722, South Korea*

(Received 5 May 2018; revised manuscript received 11 August 2018; published 10 October 2018)

Experimental verifications of cloaking, which can make objects invisible, have long been limited to single-frequency operation for relatively small objects. In this paper, we demonstrate a metamaterial cloak enabling multifrequency operation for an electrically large object, which can be robustly controlled based on an intrinsic harmonics selection condition. By designing an inhomogeneous isotropic refractive index that collimates the scattered wave path into forward direction rather than bending the propagating wave around the object exactly, the harmonics selection condition for multifrequency cloaking is naturally derived by matching the phase delay induced from the cloak medium to 2π harmonics. Then, the cloaking harmonics are controlled robustly by adjusting the size of the hidden object, which determines the phase delay inside the cloak without any extrinsic schemes such as actively controllable metamaterials. From the merit of the isotropic nature, the proposed cloak is fabricated in the three-dimensional space and verified experimentally from the reduced electromagnetic scatterings of a copper double cone. The proposed cloak employs a distinct manner, which may open a new paradigm to design multiband apparatuses such as stealth or camouflage.

DOI: 10.1103/PhysRevApplied.10.044027

An electromagnetic cloak based on the transformation optics (TO) technique [1–3], which can make an object invisible based on constitutive parameters matched with a curved space, has attracted a great deal of attention as one of the perfect stealth technologies since its invisibility performance was verified experimentally [2]. However, the main drawbacks of such a cloak are that not only is the operating bandwidth very narrow but its size is also too bulky to be applied in real applications. To address these issues, other types of cloaking techniques have been proposed based on plasmonic shells [4,5] or two-dimensional (2D) metamaterials [6,7]. Despite successful verifications, the high complexity of metamaterial design may be burdensome especially for an object that is electrically large, i.e., larger than one wavelength.

Another popular cloaking technique is the unidirectional cloak based on TO, which offers great advantages in terms of the constitutive parameters being nonsingular and/or homogeneous [8–10]. However, the experimental

verification of it is limited to a single frequency in the 2D space due to the complex anisotropic parameters [10]. The cloaks based on the balanced loss and gain [11–13], or integral imaging [13,14] may be alternative regimes. In spite of their practicality, the cloaking function based on the balanced loss and gain is lost completely when the wave is incident on the active region instead of the lossy side [12], and the structural complexity of the digital integral cloak may increase when additional materials are added to match the phases of the rays for ideal cloaking [14]. The cloak based on topology optimization has great merit that guarantees cloaking performance for multidirectional waves [15,16]. However, the fact that its total size has to be increased for dual-band cloaking performance, e.g., four times larger than that of the hidden object, remains a limitation [16]. In this study, a multifrequency unidirectional cloak for an electrically large object is proposed based on the popular quasiconformal mapping (QCM) technique [17–21] and experimentally verified in the three-dimensional (3D) space.

The QCM technique has a great advantage that preserves the isotropic nature of the cloaking material while transforming an arbitrarily shaped 2D object to a

*yongshik.lee@yonsei.ac.kr

†chengwei.qiu@nus.edu.sg

one-dimensional (1D) object. However, it is well known that the QCM technique is not suitable to the free-space cloak because the medium must be immersed in a background dielectric material, i.e., with a nonunity refractive index [10,17]. Moreover, the isotropic refractive index calculated by averaging the anisotropic refractive indices for a very small anisotropy factor α degrades the cloaking phenomena, such as the noticeable lateral beam shift for the ground-plane cloak [20] or strong forward scattering for the free-space cloak [21]. Here, α is defined by δ_x/δ_y , where δ_x and δ_y are expansion and shrink ratios of the rectangular grid along the x and y axes, respectively, compared with the grid in the virtual free space [17,20,21].

To solve the problems, a method was proposed that scales the refractive index profile of the cloak uniformly to compensate for the degradation in the cloaking performance due to the nonunity α [21]. However, the method is not applicable for electrically large objects, since α cannot be considered to be uniform across the entire structure. The long propagation path associated with the large size increases the error. This becomes much more critical when the height of the cloak is reduced for miniaturization as evidenced in Fig. 1(a), which shows the inverse relationship between α and the height of the cloak h_{cloak} . Since the shrinkage of the grid is dominantly affected by the distance between the upper and bottom boundaries of the cloaking medium, α is varying inside the cloak depending on the shape of the hidden object. The inset shows the physical space of the cloak composed with rectangular grids transformed from those of the virtual free space. The width and height of a diamond object inside the cloak are $w_{\text{obj}} = 10\lambda_0$ (200 mm) and $h_{\text{obj}} = 5\lambda_0$ (100 mm), respectively, where λ_0 is the free-space wavelength at 15 GHz. The width of the cloak is $20\lambda_0$ (400 mm).

In this paper, a design method to enhance the cloaking performance of an electrically large object is proposed. First, the refractive index profile of a miniaturized cloak designed with $h_{\text{cloak}} = 136$ mm is discretized into $6 \times 6 \text{ mm}^2$ pixels. To reduce the size, the cloak is truncated to the width of the diamond object, $w_{\text{cloak}} = 200 \text{ mm}$. The anisotropy factor α of Fig. 1(b) is calculated for each pixel, and the pixels are sectionalized such that α remains within ± 0.005 in each section. This is shown in Fig. 1(c), where the medium is sectionalized into 30 sections. Sections close to the right vertex in Fig. 1(c) are larger because the refractive index below unity in this region is approximated to unity, automatically setting α to 1.

Second, the column scaling factors β_j are multiplied to the refractive indices of the sectors in the j th column in Fig. 1(c). This is because α is affected dominantly by the shrinkage of the transformed space along the vertical direction. By scaling the refractive indices, i.e., controlling the gradient of the index profile, not only the wave path distorted by α [20] but also the phase delay inside the cloak can be optimized to diminish the scattering. To

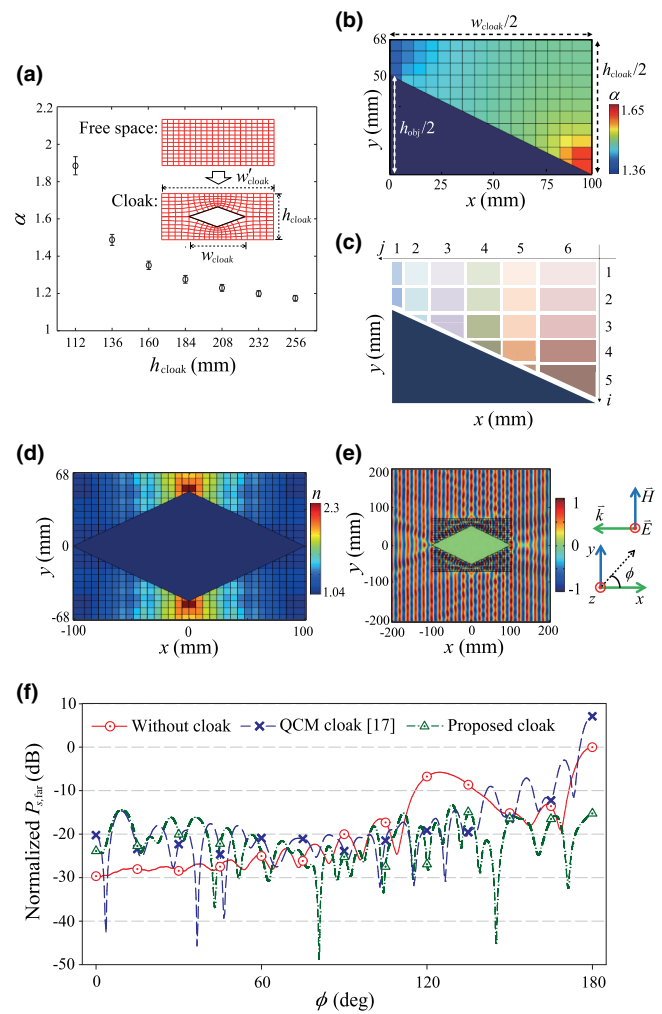


FIG. 1. Refractive index n , anisotropy factor α , and full-wave simulation results at 15 GHz of the free-space unidirectional cloak. (a) Mean and standard deviation of α vs the height of the cloak. (b) α inside the cloaking medium. (c) Rectangular sectors sectionalized by α . (d) Optimized refractive index profile. (e) Full-wave simulation of the proposed cloak. (f) Far-field scattering patterns of a diamond PEC with and without the cloak.

this end, each scaling factor β_j is determined to minimize the normalized scattering width (SW) of the diamond perfect electric conductor (PEC) at a design frequency 15 GHz. The SW is the ratio between the total scattered power and incident power intensity in the 2D space, and the normalized SW is the ratio between the SWs with and without the cloak. Next, the row scaling factors γ_i are multiplied to the refractive indices of the sectors in the i th row. The row scaling factor is determined in the same way, to compensate the distortion caused by the expansion of the transformed space along the horizontal direction. The detailed flow chart of the optimization procedure and the final scaling factors can be found in the Supplemental Material [22].

Figures 1(d) and (e) show the final refractive indices and the full-wave simulation of the proposed cloak, respectively. The plane wave propagating along the $-x$ axis with a negligible distortion verifies an excellent cloaking performance. Moreover, the far-field scattering pattern of the proposed cloak in Fig. 1(f) reveals substantial scattering reductions 15.24 and 22.34 dB in the propagating direction $\varphi = 180^\circ$ compared with those of the bare diamond PEC and the QCM cloak [17], i.e., the cloak before scaling. The scattering patterns are normalized to the peak level of the diamond PEC without the cloak. Although the cloak increases scattering in the backward direction $\varphi = 0^\circ$ due to the impedance mismatch and internal reflections [23], scattering still remains below -20 dB. The normalized SW is reduced to 0.174 with the proposed cloak, which corresponds to a 82.6% reduction in scattering.

Moreover, the invisibility can be achieved at multiple frequencies. One of the major principles of the cloak is making the phase difference 2π or a multiple of it between the waves inside and outside the medium. That is, the difference in the phase of the waves propagating through and outside the cloak at the design frequency satisfies

$$\Delta\varphi(\omega) = \int_{l_{in}} \omega n(x, y)/cdl - \int_{l_{out}} \omega/cdl = 2\pi m, \quad (1)$$

where ω is the angular frequency, $n(x, y)$ is the refractive index inside the cloak, c is the speed of light in free space, and m is an integer. The wave path inside the cloak is l_{in} while the path outside is l_{out} . By taking advantage of the large cloak based on the inhomogeneous isotropic refractive index being larger than unity, which collimates the scattered wave into the forward direction, Eq. (1) is satisfied at more than one frequency, i.e., a harmonics selection condition is derived intrinsically.

For the optimized design in Fig. 1(d), the condition $m = 4$ is satisfied at a design frequency of 15 GHz. Therefore, the medium also operates as a cloak at frequencies where $m = 3, 2, 1$, and 0, which is 12, 8, 5.2, and 2.3 GHz, respectively. The cloaking harmonics are not in a linear relationship because the refractive index profile $n(x, y)$ in Eq. (1) is inhomogeneous and the propagating paths l_{in} inside the cloak are varying at different frequencies. The number of cloaking harmonics m is calculated by subtracting phases inside and outside the cloak for each frequency that minimizes the normalized SW.

The calculated normalized SW is shown in Fig. 2(a). The results reveal that the normalized SW is a strong function of frequency, which is minimized at 12, 8, 5.2, and 2.3 GHz to 0.736, 0.852, 0.38, and 0.266, respectively. Because the proposed cloak does not utilize superluminal velocity, it is not possible to satisfy $m = 0$. However, a similar cloaking effect is achieved when the phase difference is minimized, $m \approx 0$, which occurs at 2.3 GHz.

The relatively high scatterings at 12 and 8 GHz, which correspond to frequencies of $m = 3$ and $m = 2$, respectively, are due to the discretized medium that may cause internal reflection and impedance mismatch at certain frequencies [23]. This can be mitigated by decreasing the variation of the refractive index by reducing the height of the diamond PEC h_{obj} . The refractive indices and cloaking harmonics for the different h_{obj} can be found in the Supplemental Material [22]. The cloaking performance may not be well preserved at frequencies higher than 15 GHz because the electrical size of the pixels in Fig. 1(d) is too large to control the wave path based on the gradient of the refractive index. For instance, the normalized SW remains around 1 at 17.8 GHz for $m = 5$. Figures 2(b) and 2(c) show the far-field patterns of the diamond PEC with and without the cloak at 5.2 and 2.3 GHz, which corresponds to $m = 1$ and $m \approx 0$, respectively. As demonstrated in Fig. 1(f), substantial scattering reductions by the proposed cloak are confirmed in the propagating direction, 5.46 and 15.6 dB at 5.2 GHz as well as 8.88 and 12.72 dB at 2.3 GHz compared with those of the bare diamond PEC and the QCM cloak, respectively.

Most importantly, the frequencies that satisfy Eq. (1) can be shifted by changing the path length within the cloaking medium l_{in} , which is determined by h_{obj} and/or w_{obj} . This indicates that the multiple cloaking frequencies enabled by the phase-matching condition can be controlled robustly by adjusting the size of the hidden object, which determines the phase delay inside the cloak without any extrinsic schemes such as actively controllable metamaterials [24–26]. The tuning of the cloaking harmonics can be seen in Figs. 2(d)–2(f), which show the normalized SWs at a design frequency of 15 GHz, and around the frequencies where $m = 1$ and $m \approx 0$ for various h_{obj} . Reducing h_{obj} shortens l_{in} , which increases the frequencies of $m = 1$ and $m \approx 0$. Increasing h_{obj} lengthens l_{in} , which decreases the frequencies in an opposite manner. Also, h_{obj} changes the m value at the design frequency. For instance, $m = 3$ is satisfied at a design frequency of 15 GHz when $h_{obj} = 80$ mm. The full-wave simulation results of the cloaks for various heights of the objects can be found in the Supplemental Material [22].

As shown in Figs. 2(d) and 2(e), the 3-dB cloaking bandwidths for $h_{obj} = 100$ mm, in which the normalized SWs remain below 0.5, are at most 3.9 and 6.7%, respectively. On the other hand, a much broader 3-dB cloaking bandwidth of 32.1% is confirmed at the lowest band in Fig. 2(f). The fractional bandwidth is calculated by the ratio between the bandwidth and the center frequency, which is the average of the upper and lower frequencies of the bandwidth. The changes in the bandwidths depending on the frequencies are due to the size-bandwidth product limitation [27]. The cloaking bandwidths of 1 GHz remain nearly constant in both Figs. 2(d) and 2(e), which is due to the

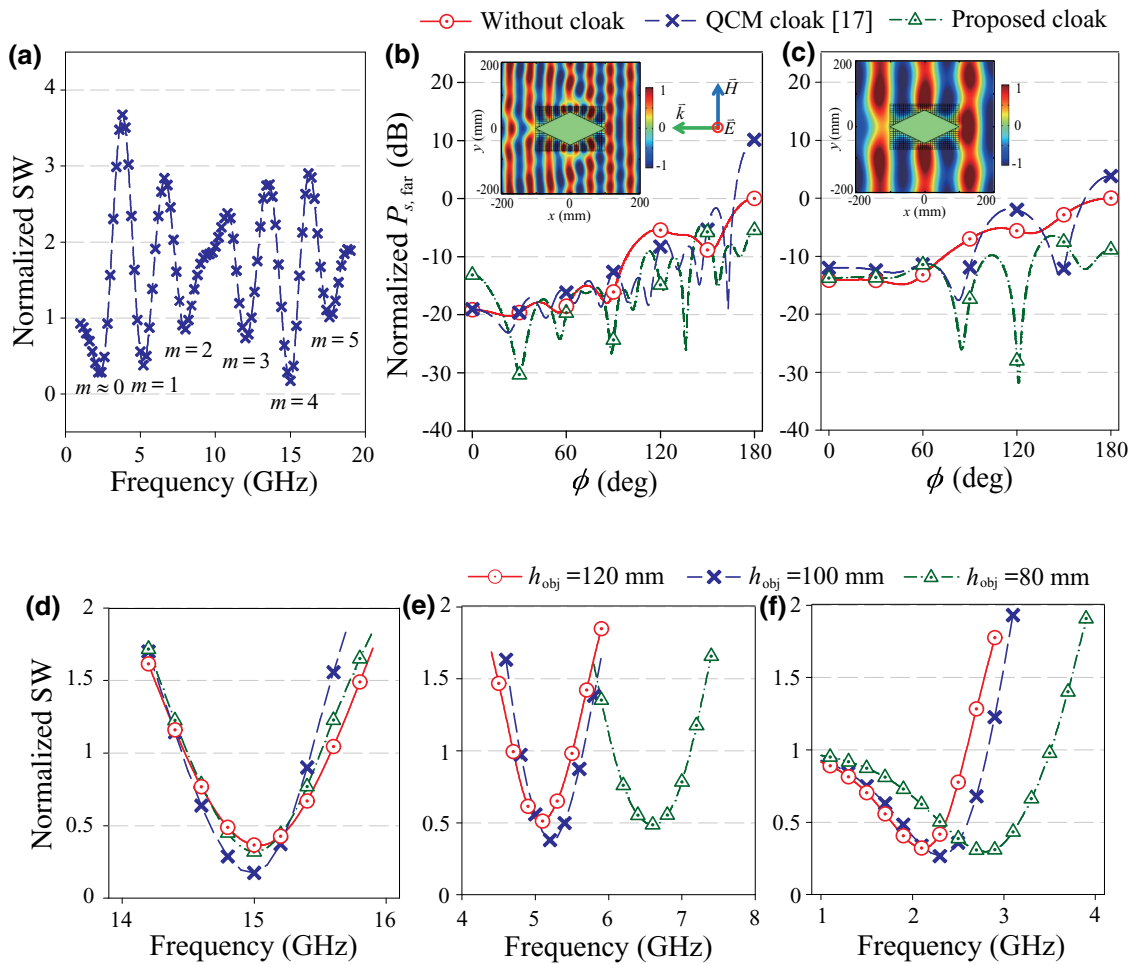


FIG. 2. Simulation results of the proposed multifrequency cloak. (a) Normalized scattering width (SW) vs frequency. Far-field scatterings of diamond PEC with and without the cloak before and after optimization at (b) 5.2 GHz and (c) 2.3 GHz. Insets: Full-wave simulations with the proposed cloak. Normalized SWs of the proposed cloaks vs frequency for various heights of the diamond objects around (d) 15 GHz, (e) 5.2 GHz, and (f) 2.3 GHz.

bandwidth being broadened by deep-scattering reduction at 15 GHz. The 3-dB cloaking bandwidth of 0.35 GHz in Fig. 2(d), which is narrower than 0.59 GHz in Fig. 2(e) for $h_{\text{obj}} = 100$ mm, is due to the bandwidth being broadened by deep-scattering reduction at a design frequency of 15 GHz. However, the relation is much more obvious when the SWs are at a similar level. For example, the 3-dB cloaking bandwidths are calculated to be 0.85, 0.72, and 0.58 GHz in Fig. 2(f) for $h_{\text{obj}} = 120$, 100, and 80 mm, respectively. This indicates that not only the cloaking frequencies but also the bandwidths can be adjusted by changing the size of the diamond object.

For experimental validation, the proposed cloak is fabricated by stacking dielectric layers in which radially symmetric cylindrical holes and fan-shaped metamaterial are embedded, as shown in Fig. 3(a). The final refractive indices in Fig. 1(d) are matched to a 3D structure by rotating them along the y axis [23,28–30]. The structural

advantage of the proposed rotational symmetric cloak is that it does not need an assumption that the structure is infinitely long along the vertical direction to the 2D space [7,24,25], the z axis in Fig. 1(e). Therefore, the proposed cloak has great merit from the perspective of practicality. Even though a limitation for the rotational symmetric structure exists in which the wave deviating from the x - y plane gradually bends along the y axis due to the gradient of the refractive index, it is heuristically verified that the major effect is still the scattering reduction with the cloak while the distortion is minor [28]. The proposed cloak has an inherent limitation that the performance is guaranteed for the transverse-electric (TE) wave. It is a common issue for the unidirectional cloaks [8–10], therefore, the improvement of polarization independence is out of the scope of this paper and remains as a future work. For each layer of the cloak, a FR4 substrate is used, which has a refractive index of 2.11 and dielectric loss tangent

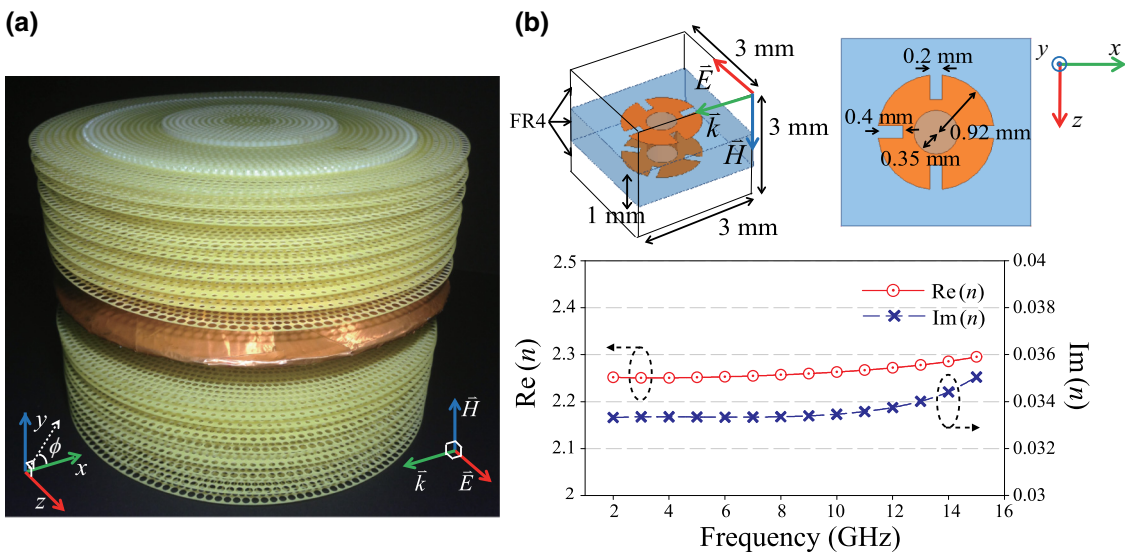


FIG. 3. 3D unidirectional cloak consisting of dielectric layers with holes and embedded fan-shaped metamaterial. (a) Fabricated cloak. (b) Real and imaginary parts of effective refractive index of metamaterial vs frequency. Top-left panel: A cubic unit cell of metamaterial. Top-right panel: Dimensions of copper patch.

of 0.029. Simulation results of a drilled-hole unit cell and the photographs of a fabricated layer can be found in the Supplemental Material [22].

Figure 3(b) shows the effective refractive index of the proposed metamaterial in a broad bandwidth. It is designed to achieve a refractive index of 2.29, which is higher than that of the FR4 substrate at 15 GHz based on an artificial electric dipole moment [31–34]. The unit cell of the metamaterial is shown in Fig. 3(b). The structure is composed of two fan-shaped copper patches connected via a hole and placed between two FR4 layers, which are rotated by 45° with respect to each other. From this configuration, a quasi-isotropic characteristic can be achieved. The simulations for different polarizations are summarized in the Supplemental Material [22].

The effect of loss in the fabricated cloak is twofold: it deteriorates the cloaking performance, and at the same time, it reduces the backward scattering [9]. From Fig. 4(a), it can be confirmed that the backward scattering is lower for the lossy cloak than the lossless counterpart. Although the loss increases the forward scattering at a design frequency of 15 GHz, electromagnetic invisibility is maintained, as evidenced by the normalized SW of 0.351. This is also the case at other frequencies, as evidenced in Figs. 4(b) and 4(c). Although scattering is higher for the lossy cloak, the normalized SWs are still much less than one, 0.42 and 0.273, at frequencies of 5.2 and 2.3 GHz, respectively.

Figures 4(d)–4(f) show the measured far-field scatterings of a copper double cone with and without the cloak at 15.2, 5.7, and 2.3 GHz, respectively, where the normalized scattering cross sections (SCS) are minimized. The

3D normalized SCS is defined in the same way as the normalized SW is defined. The shifted frequencies compared with those of the simulation are due to the issues of the accuracy of drilling holes inside the substrates as well as the coupling [10] and the dispersion of the metamaterials. The scattering patterns are measured in the azimuthal x - y plane for the incident angle $\phi = 0^\circ$ in the range of $\phi = 60^\circ$ to 180° with a 2° step. The minimum angle for the measurement is determined by the smallest angle between the rotational arms of the transmitting and receiving antennas, which are covered with microwave absorbers. A detailed description of the measurement system is summarized in the Supplemental Material [22].

Table I summarizes the simulated 2D normalized SWs and measured 3D normalized SCSs. In addition to the structural difference between the 2D and the rotationally symmetric 3D cloaks, there exist major issues that cause the differences between the measured and simulated results. First, $3 \times 6 \times 3 \text{ mm}^3$ cuboid unit cells along the x - y - z axes [22], which are used to match the refractive indices in the range of $|x| \geq 42 \text{ mm}$ of Fig. 1(d), may cause deterioration in controlling the wave path along the y axis because the thickness along the y axis may not be sufficiently thin at the high frequency. Second, an approximation of refractive indices less than 1.05 to 1 in the range of $|y| \leq 20 \text{ mm}$ may deteriorate the function of controlling the wave at the edge, i.e., $|x| = \pm 100 \text{ mm}$, of the copper double cone. Even though there exists a discrepancy between the simulated and measured results at the highest frequency 15 GHz due to error factors enlarged by the long-propagation path in the wavelength, the normalized SCS less than 1 still indicates

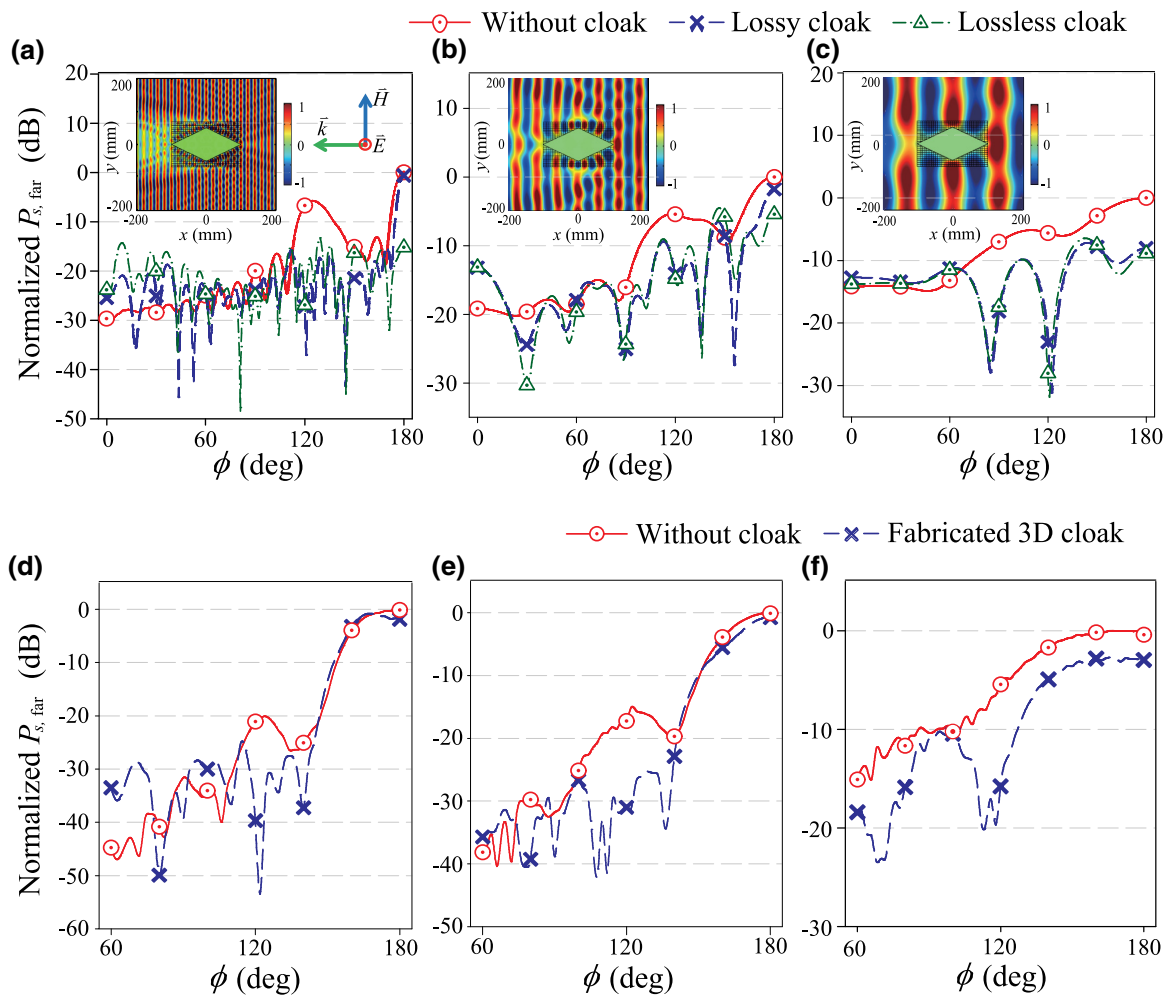


FIG. 4. Simulated and measured far-field scatterings normalized by the peak levels of the bare objects. Simulations of a diamond PEC with and without lossless or lossy cloaks at (a) 15 GHz, (b) 5.2 GHz, and (c) 2.3 GHz. Insets: Full-wave simulations with the lossy cloak. Measurements of a copper double cone with and without the fabricated cloak at (d) 15.2 GHz, (e) 5.7 GHz, and (f) 2.3 GHz.

appreciable scattering reduction. Besides, very large reductions in the side lobes in Figs. 4(d)–4(f), which are well matched with the expected simulation results verify the function of collimating the scattered wave in the forward direction.

In conclusion, a multifrequency unidirectional cloak is proposed based on an intrinsic harmonics selection condition of the optimized inhomogeneous isotropic

cloak medium. The cloaking harmonics can be controlled robustly by changing the phase delay inside the cloak resorting to the size of the hidden object. From the full-wave simulations as well as the experimental results that verify the appreciable scattering reductions, the multifrequency cloaking performance is demonstrated. The proposed method may open a new avenue to apply the cloak for stealth or camouflage, which can maintain the functionalities for multiband radar signals by controlling the size of the object to shift the center frequency of each band as well as satisfy the bandwidth conditions.

TABLE I. Comparison of full-wave simulated and measured cloaking performances.

Frequency (GHz)	15	5.2	2.3
Simulated			
(2D normalized scattering width)	0.351	0.42	0.273
Frequency (GHz)	15.2	5.7	2.3
Measured			
(3D normalized scattering cross section)	0.918	0.751	0.474

ACKNOWLEDGMENTS

This work is supported by the Yonsei University Future-leading Research Initiative of 2015 (Grant No. 2015-22-0066) and the Center for Advanced Meta-Materials (CAML) funded by the Ministry of Science and ICT of

the Korea government (Global Frontier Project Grant No. 2014M3A6B3063700).

-
- [1] J. B. Pendry, D. Schurig, and D. R. Smith, Controlling electromagnetic fields, *Science* **312**, 1780 (2006).
- [2] D. Schurig, J. J. Mock, B. J. Justice, S. A. Cummer, J. B. Pendry, A. F. Starr, and D. R. Smith, Metamaterial electromagnetic cloak at microwave frequencies, *Science* **314**, 977 (2006).
- [3] A. Nicolet, and F. Zolla, Cloaking with curved spaces, *Science* **323**, 46 (2009).
- [4] A. Alù, and N. Engheta, Multifrequency Optical Invisibility Cloak with Layered Plasmonic Shells, *Phys. Rev. Lett.* **100**, 113901 (2008).
- [5] C.-W. Qiu, L. Gao, J. D. Joannopoulos, and M. Soljacic, Light scattering from anisotropic particles: Propagation, localization, and nonlinearity, *Laser Photon. Rev.* **4**, 268 (2010).
- [6] A. Alù, Mantle cloak: Invisibility induced by a surface, *Phys. Rev. B* **80**, 245115 (2009).
- [7] J. C. Soric, A. Monti, A. Toscano, F. Bilotti, and A. Alù, Multiband and wideband bilayer mantle cloaks, *IEEE Trans. Antennas Propag.* **63**, 3235 (2015).
- [8] W. X. Jiang, T. J. Cui, X. M. Yang, Q. Cheng, R. Liu, and D. R. Smith, Invisibility cloak without singularity, *Appl. Phys. Lett.* **93**, 194102 (2008).
- [9] Y. Luo, J. Zhang, H. Chen, L. Ran, B.-I. Wu, and J. A. Kong, A rigorous analysis of plane-transformed invisibility cloaks, *IEEE Trans. Antennas Propag.* **57**, 3926 (2009).
- [10] N. Landy, and D. R. Smith, A full-parameter unidirectional metamaterial cloak for microwaves, *Nat. Mater.* **12**, 25 (2013).
- [11] G. Castaldi, S. Savoia, V. Galdi, A. Alù, and N. Engheta, PT Metamaterials via Complex-Coordinate Transformation Optics, *Phys. Rev. Lett.* **110**, 173901 (2013).
- [12] D. L. Sounas, R. Fleury, and A. Alù, Unidirectional Cloaking based on Metasurfaces with Balanced Loss and Gain, *Phys. Rev. Appl.* **4**, 014005 (2015).
- [13] M. McCall, J. B. Pendry, V. Galdi, Y. Lai, S. A. R. Horsley, J. Li, J. Zhu, R. C. Mitchell-Thomas, O. Quevedo-Teruel, P. Tassin, V. Ginis, E. Martini, G. Minatti, S. Maci, M. Ebrahimpour, Y. Hao, P. Kinsler, J. Gratus, J. M. Lukens, A. M. Weiner, U. Leonhardt, I. I. Smolyaninov, V. N. Smolyaninova, R. T. Thompson, M. Wegener, M. Kadic, and S. A. Cummer, Roadmap on transformation optics, *J. Opt.* **20**, 063001 (2018).
- [14] J. S. Choi, and J. C. Howell, Digital integral cloaking, *Optica* **3**, 536 (2016).
- [15] Y. Urzhumov, N. Landy, T. Driscoll, D. Basov, and D. R. Smith, Thin low-loss dielectric coatings for free-space cloaking, *Opt. Lett.* **38**, 1606 (2013).
- [16] N. Kishimoto, K. Izui, S. Nishiwaki, and T. Yamada, Optimal design of electromagnetic cloaks with multiple dielectric materials by topology optimization, *Appl. Phys. Lett.* **110**, 201104 (2017).
- [17] J. Li, and J. B. Pendry, Hiding Under the Carpet: A New Strategy for Cloaking, *Phys. Rev. Lett.* **101**, 203901 (2008).
- [18] H. F. Ma, W. X. Jiang, X. M. Yang, X. Y. Zhou, and T. J. Cui, Compact-sized and broadband carpet cloak and free-space cloak, *Opt. Express* **17**, 19947 (2009).
- [19] E. Kallos, C. Argyropoulos, and Y. Hao, Ground-plane quasicloaking for free space, *Phys. Rev. A* **79**, 063825 (2009).
- [20] B. Zhang, T. Chan, and B.-I. Wu, Lateral Shift Makes a Ground-Plane Cloak Detectable, *Phys. Rev. Lett.* **104**, 233903 (2010).
- [21] Y. Kim, I. Seo, I.-S. Koh, and Y. Lee, Design method for broadband free-space electromagnetic cloak based on isotropic material for size reduction and enhanced invisibility, *Opt. Express* **24**, 22708 (2016).
- [22] See Supplemental Material at <http://link.aps.org/supplemental/10.1103/PhysRevApplied.10.044027> for additional information on the design flow chart, full-wave simulation results of the cloaks for various heights of the diamond objects, refractive indices of metamaterials, fabricated structure, and the measurement system.
- [23] N. Wang, Y. Ma, R. Huang, and C. K. Ong, Far field free-space measurement of three dimensional hole-in-Teflon invisibility cloak, *Opt. Express* **21**, 5941 (2013).
- [24] P.-Y. Chen, C. Argyropoulos, and A. Alù, Broadening the Cloaking Bandwidth with Non-Foster Metasurfaces, *Phys. Rev. Lett.* **111**, 233001 (2013).
- [25] S. Liu, H.-X. Xu, H. C. Zhang, and T. J. Cui, Tunable ultra-thin mantle cloak via varactor-diode-loaded metasurface, *Opt. Express* **22**, 13403 (2014).
- [26] R. Fleury, F. Monticone, and A. Alù, Invisibility and Cloaking: Origins, Present, and Future Perspectives, *Phys. Rev. Appl.* **4**, 037001 (2015).
- [27] H. Hashemi, C.-W. Qiu, A. P. McCauley, J. D. Joannopoulos, and S. G. Johnson, Diameter-bandwidth product limitation of isolated-object cloaking, *Phys. Rev. A* **86**, 013804 (2012).
- [28] N. I. Landy, N. Kundtz, and D. R. Smith, Designing Three-Dimensional Transformation Optical Media using Quasi-conformal Coordinate Transformations, *Phys. Rev. Lett.* **105**, 193902 (2010).
- [29] H. F. Ma, and T. J. Cui, Three-dimensional broadband ground-plane cloak made of metamaterials, *Nat. Commun.* **1**, 21 (2010).
- [30] W. X. Jiang, S. Ge, T. Han, S. Zhang, M. Q. Mehmood, C.-W. Qiu, and T. J. Cui, Shaping 3D path of electromagnetic waves using gradient-refractive-index metamaterials, *Adv. Sci.* **3**, 1600022 (2016).
- [31] J. B. Pendry, A. J. Holden, W. J. Stewart, and I. Youngs, Extremely Low Frequency Plasmons in Metallic Mesostructures, *Phys. Rev. Lett.* **76**, 4773 (1996).
- [32] J. Shin, J.-T. Shen, and S. Fan, Three-Dimensional Metamaterials with an Ultrahigh Effective Refractive Index Over a Broad Bandwidth, *Phys. Rev. Lett.* **102**, 093903 (2009).
- [33] M. Choi, S. H. Lee, Y. Kim, S. B. Kang, J. Shin, M. H. Kwak, K.-Y. Kang, Y.-H. Lee, N. Park, and B. Min, A terahertz metamaterial with unnaturally high refractive index, *Nature* **470**, 369 (2011).
- [34] Y. Kim, M. Kim, Y. Lee, J. Park, I. Seo, and I.-S. Koh, Broadband polarisation-independent metamaterial based on modified ELC structure, *Int. J. Nanotechnol.* **13**, 299 (2016).